GTP-17-1057

AN IMPROVED RATE OF HEAT RELEASE MODEL FOR MODERN HIGH SPEED DIESEL ENGINES

Peter G. Dowell, Sam Akehurst, Richard D. Burke

Dept. of Mechanical Engineering, University of Bath, Bath, UK, email: R.D.Burke@bath.ac.uk

Key Words: Combustion Modelling, Rate of Heat Release, Ignition Delay, Rate of Injection

ABSTRACT

To meet the increasingly stringent emissions standards, Diesel engines need to include more active technologies with their associated control systems. Hardware-in-the-Loop (HiL) approaches are becoming popular when the engine system is represented as a real-time capable model to allow development of the controller hardware and software without the need for the real engine system. This paper focusses on the engine model required in such approaches. A number of semi-physical, zero-dimensional combustion modelling techniques are enhanced and combined into a complete model, these include- ignition delay, pre-mixed and diffusion combustion and wall impingement. In addition, a fuel injection model was used to provide fuel injection rate from solenoid energizing signals.

The model was parameterized using a small set of experimental data from an engine dynamometer test facility and validated against a complete data set covering the full engine speed and torque range. The model was shown to characterize Rate of Heat Release (RoHR) well over the engine speed and load range. Critically the wall impingement model improved R^2 value for maximum RoHR from 0.89 to 0.96. This reflected in the model's ability to match both pilot and main combustion phasing, and peak heat release rates derived from measured data. The model predicted indicated mean effective pressure and maximum pressure with R^2 values of 0.99 across the engine map. The worst prediction was for the angle of maximum pressure which had an R^2 of 0.74. The results demonstrate the predictive ability of the model, with only a small set of empirical data for training – this is a key advantage over conventional methods. The fuel injection model yielded good results for predicted injection quantity (R^2=0.99), and enables the use of the RoHR model without the need for measured rate of injection.

NOMENCLATURE

Abbreviations

AFR	Air-fuel-ratio
ATDC	After top dead centre
BDC	Bottom dead centre
BMEP	Brake mean effective pressure
BTDC	Before top dead centre
CA	Crank Angle
ECU	Engine control unit
EGR	Exhaust gas recirculation
EOC	End of combustion
EOI	End of injection
gIMEP	Gross indicated mean effective pressure
HiL	Hardware-in-the-loop
HR	Heat release
HSDI	High-speed direct injection
IMEP	Indicated mean effective pressure
LTC	Limiting torque curve
MAF	Mass airflow
MCC	Mixing controlled combustion
nIMEP	Net indicated mean effective pressure
PMEP	Pumping mean effective pressure
R^2	Coefficient of determination
RMSE	Residual mean square error
ROI	Rate of injection
RoHR	Rate of heat release
RT	Real-time
SD	Standard deviation
SFC	Specific fuel consumption
SOC	Start of combustion
SOI	Start of injection
SSE	Sum of square errors
TDC	Top dead centre

Mathematical Symbols

A	Area	m^2
a_{1-12}	Fitted constants	-
AFR	Air-to fuel ratio	
C_{arr}	Arrhenius model constant (Fitted)	
C_c	Contraction coefficient	
C_d	Drag coefficient	-
C_{diss}	Dissipation constant for (fitted)	s^{-1}
C_{mag}	Magnussen model constant	
C_{mod}	Chmla Combustion model constant (fitted)	J/kg/°CA
c_p	Specific heat capacity at constant pressure	J/kgK
C_{turb}	Turbulence generation constant (fitted)	
c_v	Specific heat capacity at constant volume	J/kgK
C_{wall}	Wall impingement model parameter (fitted)	
d	diameter	m
E	Energy	J
f	Function	-
H	Enthalpy	J
h	Specific enthalpy	J/kg
h_c	Convective heat transfer coefficient	W/m^{2}K
k	Turbulence density	J/kg
L	Length	m
LCV	Lower calorific value	
m	Mass	kg
$\dot{m}$	Mass flow	kg/s
N	Speed	rev/min
n	Polytropic index	-
p	pressure	bar or Pa
Q	Heat Energy	J
q	Heat flux	W/m^2
R	Gas constant	J/kgK
r	Radius	m
R^2	Coefficient of determination	-
T	Temperature	K or °C
T	Time	s
U	Internal energy	J
V	Volume	m^3
v	Velocity	m/s
W	Work	J
x	Fuel mass share	-

Greek Symbols

α_{max}	Point of maximum pressure	°CA ATDC
γ	Polytropic coefficient (ratio of specific heats)	-
η	Efficiency	-
θ	Crank angle	rad
θ_{max}	Point of maximum heat release	°CA ATDC
λ	Stoichiometric ratio	
π	Pi	-
ρ	Density	kg/m^3
σ	Emissivity	kW/m^{2}k^4
τ	Time constant	

Subscripts

$avail$	Available
bb	Blow-by
Ch	Chemical
c	Combustion

cyl	Cylinder, Cylinder charge
diff	Diffusion combustion
eng	Engine
EOI	End of Injection
ex	Exhaust valve
evap	Evaporated
f	Fuel
HT	Heat Transfer
ID	Ignition Delay
in	Inlet Valve
inj	Injected
liqu	Liquid
noz	Injector nozzle
Ph	Physical
Pilot	From the pilot injection
pre	Pre-ignition
Rail	In the high pressure fuel rail
SOC	Start of Combustion
SOI	Start of Injection
stoich	Stoichiometric
vap	Vapourized

1   INTRODUCTION

Diesel engine design is becoming ever more complex in order to meet increasingly stringent emissions standards: some recent examples are the use of high and low pressure exhaust gas recirculation (EGR) and multi-stage turbochargers with variable geometry turbines. With current and future drive cycles running from cold start and containing harsher transients, control strategies can no longer be developed under steady-state conditions. This means the task of developing a capable control strategy has become more demanding and time consuming.. Hardware-in-the-loop (HiL) techniques have been spearheaded by manufacturers by replacing engine hardware with real time models in an effort to reduce time spent on dynamometer testing and reduce overall development times. Nevertheless, current HiL models tend to rely on significant levels of empirical data to meet sufficient levels of accuracy which limits their usefulness in controller design as they are typically not available until a significant volume of calibration test data is available.

This paper aims to address the limitations of current HiL models by combining a number of state-of-the-art zero-dimensional combustion modelling techniques and applying a global parameterisation with only a small amount of experimental data. The work focusses on enhancing Rate of Heat Release prediction through consideration of fuel injection, ignition delay; pre-mixed combustion; wall impingement and pilot combustion. This new RoHR model would be used in conjunction with a single zone zero dimensional cylinder model.

2   BACKGROUND

A vital element of transient engine modelling is the accurate prediction of combustion behavior, since the progression of the Rate of Heat Release (RoHR) primarily dictates the engine performance and emissions [1]. The RoHR is a key input to the single zone cylinder models which undertake an energy balance on combustion, work, heat and enthalpy transfers to calculate in-cylinder pressure and temperature. These are vital for predicting engine performance but also interact with the turbocharger and Exhaust Gas Recirculation (EGR) models [2]. A recent review of engine modelling has shown this to be one of the main weaknesses compared to more computationally demanding 1D or multidimensional in-cylinder models. [3].

For controller design, it is essential that model run times are kept to a minimum to provide real time capabilities. By taking a zero-dimensional approach to RoHR modelling, model execution times can be reduced significantly [4]. Several techniques exist for accurately predicting in-cylinder pressure and RoHR in an efficient way, including neural networks [5, 6-8]; Wiebe methods (shape functions) [4, 9-12]; and phenomenological methods [13-15] such as mixing controlled combustion models [13]. These three types will be briefly described below.

2.1   Neural Networks

As highly non-linear mathematical functions, Neural networks are black-box models and therefore mask the underlying physical processes. For combustion modelling, this can be seen as a disadvantage as it prevents any analysis of the phenomena underpinning the resulting performance. Since neural nets have difficulty in making predictions outside of the range of training data, an exhaustive set of training and validation data are required owing to the many degrees of freedom associated with modern DI combustion [4]. Therefore, in order for the Neural network to act as predictor, it must be trained with empirical data covering the specific range of interest meaning large amounts of experimental data are required which undermines the argument for HiL based controller design.

2.2   Wiebe Models

Wiebe models describe the apparent fuel burning rate by fitting a Wiebe function to experimentally derived data. One common form of Wiebe model is the double Wiebe model suggested by Watson [10] which captures the pre-mixed and diffusion phases of Diesel combustions; however, this cannot represent split injection strategies (e.g. pilot and post injections), therefore making its use in modern diesel engines limited. A more general multi-Wiebe method is described in [16].

By introducing additional Wiebe curves, pre and post combustion events can be modelled (see figure 1). However, this increases the modelling effort considerably, since for each Wiebe curve, several parameters need to be tuned for each operating condition. As with neural networks, this can lead to problems of dimensionality [4], increasing the time taken to parameterise a model due to the quantity of data required.

1.3   Mixing controlled combustion

Chmela & Orthaber [17] hypothesized that the rate of heat release could be related the product of two parameters; the mixing rate and the fuel availability as described in equation 1.

$$\frac{dQ_{cyl}}{d\theta} = C_{mod} \cdot LCV \left(m_f - \frac{Q_{cyl}}{LCV} \right) \cdot f_{mixing} \qquad (1)$$

Based on the observation that over 90% of the contribution to turbulent energy density input prior to combustion was due to fuel injection [17, 18] and that diffusion combustion is very closely related to the rate of injection (ROI) [1, 14, 15, 17, 19], they proposed that the mixing rate, and therefore RoHR, could be derived from the rate of injection.

They proposed simplifying Magnussen's theory of turbulent burning [20], replacing the term with a rate proportional to the square root of the kinetic energy density and a characteristic length derived from the instantaneous cylinder volume [17] (equation 2). k is defined later in equation 13.

$$f_{mixing} = \frac{\sqrt{k}}{\sqrt[3]{V_{cyl}}} \qquad (2)$$

However, as described by Dec [21], combustion in a modern DI engine can be described by two distinct phases: a rich, pre-mixed phase due to ignition delay, followed by the stoichiometric diffusive phase. As a result, this fails to describe combustion fully, especially at part-load where ignition delay and pre-mixed combustion are more prevalent, representing significant proportions of the total heat release [17, 18, 22, 23]. In addition to this, at high load on small displacement engines, interaction with the cylinder wall and combustion bowl can cause significant deviations from the predicted RoHR using the original MCC model [17, 18].

In this paper we seek to enhance the mixing controlled combustion model by introducing sub-models of, ignition delay, premixed combustion, wall impingement and pilot injection. The aim of this work is to parameterize these physical models using a small subset of engine dynamometer data that enables good prediction over a broad range of engine operating conditions.

3   COMBUSTION MODELLING APPROACH

Considering the engine cylinder as a control volume and applying the conservation of energy, the change in internal energy of the gases in the cylinder can be equated as the sum of the heat released from combustion, the heat lost to the combustion chamber walls, the work transfer to the piston and the net enthalpy flow from valve opening and blow-by (equation 3) [24].

$$\dot{U} = \dot{Q}_c - \dot{Q}_{HT} - \dot{W} + \dot{H}_{in} - \dot{H}_{ex} - \dot{H}_{bb} \qquad (3)$$

It is assumed that the mass trapped in the cylinder is at a homogeneous temperature which can be related to the internal energy U through the specific heat capacity. The perfect gas law can then be used to derive the instantaneous pressure in the cylinder and the equation solved on a crank angle basis. Whilst each of the terms in equation 3 deserve careful attention, the work in this paper will focus on modelling the heat release due to combustion, $\dot{Q}_c$. It will be decomposed into premixed and diffusive components (equation 4) and applied to pilot and main injections. This will be described in detail in section 3.1.

$$\dot{Q}_c = \frac{dQ_{pre}}{dt} + \frac{dQ_{diff}}{dt} \qquad (4)$$

3.1   Combustion Models

In this section the six key physics based models used to describe the Diesel fueling and combustion process are described. The combustion model is composed of:

- An ignition delay model
- A premixed combustion model
- A diffusion combustion model

- A wall impingement model

- A pilot combustion model

- A fuel injection model

Figure 2 shows the contributions of these models at an arbitrary engine operating point including a single pilot and main injection event. Finally the fueling process is modelled using an empirical approach to predict the rate of fuel injection from the injector driver controller.

3.1.1 Ignition delay model

The prediction of combustion delay is of great importance to the combustion model because of its impact on the shaping of the rate of heat release following the delay period [24]. Figure 3 illustrates the effect of ignition delay on modelled main combustion. When SOC is predicted early, the pre-mixed combustion is under predicted, and diffusion combustion is over-predicted, see figure 3 (b). This is because ignition delay defines the portion of fuel dedicated to either pre-mixed, or diffusion combustion, altering the RoHR profile significantly.

The ignition delay period is a function of both a physical delay (τ_{ph}) associated with fuel spray characteristics such as vaporization and mixing and a chemical delay (τ_{ch}) that cover pre-reactions which occur prior to ignition [25]. The ignition delay time constant is a sum of these two, and is inversely proportional to the reaction rate. Equation 5 represents the integral between SOI and SOC and constants are scaled so that SOC occurs when the equation reaches unity.

$$\int_{SOI}^{SOC} \frac{1}{\tau_{ID}} dt = 1, \ Where \ \tau_{ID} = \tau_{ph} + \tau_{ch} \qquad (5)$$

Numerous authors have used a correlation based on an Arrhenius expression [25] to describe the chemical delay as shown in Equation 6. However, the works of Chmela et al [22, 25] suggest that this alone is not enough to describe the process in a modern, high-pressure direct injection engine. In this case, the approach taken by Magnussen [20] is used to describe the effect of the turbulent energy density k which is increased by injection as shown in equation 7. The reaction rates are scaled by the concentrations of fuel and oxygen. These are calculated by dividing the fluid mass

by the mixture volume V_{mix}, which is calculated as the sum of the volume of fuel and air based on a fixed air-fuel-ratio, and the cylinder gas density derived from spatially averaged in-cylinder pressure.

$$\frac{1}{\tau_{ch}} = C_{arr}c_f c_0 e^{-\frac{a_1 T_i}{T}} \qquad (6)$$

$$\frac{1}{\tau_{ph}} = C_{mag}c_f \frac{\sqrt{k}}{\sqrt[3]{V_{cyl}}} \qquad (7)$$

$$Where\ c_f = \frac{m_f}{V_{mix}}, \qquad c_o = \frac{0.232 m_{cyl}}{V_{mix}}$$

$$and\ V_{mix} = m_f \left(\frac{1}{\rho_{F,vap}} + \frac{\lambda(AFR)_{stoich}}{\rho_{cyl}} \right)$$

Figure 4 compares the ignition delay predicted by the Magnussen equation, the Arrhenius equation, and the resultant, combined rate against measured data. Although the ignition delay models are presented as curves for clarity, these represent the calculated ignition delays at the particular measured points. This explains the shape of these curves in the region of 800-900bar rail pressure and the graph should not be interpreted as a absolute relationship between rail pressure and ignition, but rather a convenient way of presenting model and experimental agreement against a meaningful physical variable. Measured ignition delay was calculated from experimental data as the time between start of injection (SOI) and start of combustion (SOC). SOI was determined from the injector model detailed below. SOC was determined differently for each injection:

- Pilot combustion was found using the method described in [25, 27] by taking the second differential of in-cylinder pressure, and finding when it crossed a significant threshold

- Main combustion could not be defined using the same method as pilot combustion as the additional noise caused by pilot combustion masks the main combustion event. In addition to this, the main combustion event has a smaller pre-mixed portion and is dominated by diffusion combustion resulting in a lower rate of pressure change which is harder to detect. Consequently main combustion SOC was determined through a threshold on RoHR.

It shows that the Magnussen rate over-estimated the decrease in ignition delay with increasing rail pressure, whereas the Arrhenius rate under-estimated the variation.

This is a logical conclusion following comparison with the equations, since the Magnussen rate is dependent on the kinetic energy density which is a function of rail pressure, whereas the Arrhenius rates is dependent on oxygen concentration and cylinder temperature which do not increase as much as the rail pressure with increasing load.

By combining both these rates the sum of the chemical and physical effects are accounted for, yielding the resultant rate which matches the measured data closely.

3.1.2 Pre-mixed combustion model

At part-load conditions, the combustion process becomes more complex, since a large proportion of the fuel is burnt during a pre-mixed reaction [22, 23, 26, 28, 29]. Lower rail pressures and in-cylinder temperatures cause auto-ignition to be delayed, meaning more fuel is mixed with air before combustion occurs, to a higher proportion of combustion being pre-mixed.

Equation 8 summarizes how pre-mixed combustion is described by an Arrhenius rate with a quadratic term containing the elapsed time since SOC to describe the initial burn rate, which progresses in a similar fashion to a spark ignition flame front [22, 26]:

$$\frac{dQ_{pre}}{dt} = a_2 c_o e^{-a_3 \frac{T_a}{T_{cyl}}} m_{pre,avail}^2 LCV (t - t_{SOC})^2 \qquad (8)$$

Where T_a is the activation temperature and the mass of fuel available for premixed combustion is defined as:

$$m_{pre,avail} = \begin{cases} x_{pre} \int\limits_{SOI}^{\theta} dm_{f,inj} - \dfrac{Q_{pre}(t)}{LCV} & \theta < \theta_{SOC} \\ 0 & \theta \geq \theta_{SOC} \end{cases}$$

x_{pre} is the portion of the fuel dedicated to pre-mixed combustion during the ignition delay period. To avoid unnecessary complexity, or reliance on additional empirical data, these were assumed to be constant for all operating conditions.

3.1.3 Diffusion Combustion Model

The diffusion combustion model is equivalent to the original MCC model reported by Chmela et al [17] with additional equations describing the allocation of fuel from the ignition delay period, and the delay caused by evaporation. It is proposed that combustion is a function of fuel availability and mixing rate [22, 23]:

$$\frac{dQ_{diff}}{dt} = C_{mod} \cdot LCV \cdot m_{f,diff,avail} \left(\frac{\sqrt{k}}{\sqrt[3]{V_{cyl}}} \right) \qquad (9)$$

Available fuel $m_{f,diff,avail}$ can be described as that which has evaporated from the liquid pool dedicated to the diffusion model [23] as detailed in equations 10-12

$$m_{f,diff,avail} = \int_{SOI}^{\theta} dm_{f,diff,evap} - \frac{Q_{diff}}{LCV} \qquad (10)$$

$$\frac{dm_{f,diff,evap}}{d\theta} = \frac{1}{6N_{eng}} \int_{SOI}^{\theta} \frac{T_{cyl}^{3.3} k}{C_{evap} d_{noz}} m_{f,diff,liqu} \qquad (11)$$

Equation 12 describes that prior to SOC a portion of liquid fuel is dedicated to the diffusion model, initiating the evaporation process which draws from the liquid pool. Once combustion has started, it is assumed that any additional fuel injected is added to the liquid diffusion fuel pool [22, 26].

$$m_{f,diff,liqu}$$

$$= \begin{cases} (1 - x_{pre}) \int_{SOI}^{\theta} dm_{f,inj} - m_{f,diff,evap} & \theta < \theta_{SOC} \\ \int_{SOC}^{\theta} dm_{f,inj} - m_{f,diff,evap} & \theta \geq \theta_{SOC} \end{cases} \qquad (12)$$

Equation 13 shows how turbulent energy density k is a function of the energy in the cylinder E_u, derived from the energy input from the injection process E_i :

$$k = \frac{E_u}{m_f \left(1 + \lambda_{diff} AFR_{stoich} \right)} \qquad (13)$$

The rate of change in energy is defined as the difference between that input into the system and energy dissipated [17]:

$$\frac{dE_u}{d\theta} = \frac{dE_i}{d\theta} - \frac{dE_{diss}}{d\theta} \qquad (14)$$

Energy input from the injection is described in equation 15, and the energy dissipation rate is described in equation 16:

$$\frac{dE_i}{d\theta} = C_{turb} 18\rho_F \left(\frac{N_{eng}}{C_d A_{noz}}\right)^2 \left(\frac{dm_f/d\theta}{\rho_f}\right)^3 \qquad (15)$$

$$\frac{dE_{diss}}{d\theta} = -\frac{C_{diss}}{6N_{eng}} E_u \qquad (16)$$

3.1.4 Wall impingement Model

At high loads, the MCC model tends to overestimate RoHR after TDC during fuel injection, but under-predicts RoHR after the EOI (see figure 13c). As a result, measured RoHR appears to lag behind the model, picking up later during the expansion stroke.

This effect is hypothesized to be a result of the injected fuel not burning immediately, but being stored and burnt later [17]. In [18], it was observed that this effect was more apparent in small sized engines (of 2 liters or less), at loads over 50%. It was proposed that this effect could be due to wall impingement slowing the rate of energy input into the system, and thus the RoHR.

A correction for wall impingement was suggested in [18] based on the momentum lost at the wall at the time of impingement, where energy input into the cylinder is modified by an additional parameter C_{wall}, see equation 17.

$$\frac{dE_i}{d\theta} = C_{wall} \cdot C_{mod} \cdot LCV \cdot m_{f,diff,avail} \left(\frac{\sqrt{k}}{\sqrt[3]{V_{cyl}}}\right) \qquad (17)$$

Equation 18 shows how in engines of small bore sizes, combustion is decelerated when the spray reaches the wall at a spray penetration $s = d_{cyl}/2$ from the injector.

$$C_{wall} = \begin{cases} \left(\dfrac{v_{wall}}{v_{free}}\right)^2 & s \geq \dfrac{d_{cyl}}{2} \\[2ex] 1 & s < \dfrac{d_{cyl}}{2} \end{cases} \tag{18}$$

$$Where \; s = \sqrt{8 C_d v_{inj} d_{inj} t} \left(\frac{294}{T_{cyl}}\right)^{1/4}$$

When the spray meets the wall, there is a continuous loss of momentum. This can be described as a loss proportional to the square of the ratio between the free velocity v_{free} and the velocity of the jet once it has met the wall v_{wall}. These are defined in equations 19 and 20 respectively.

$$v_{free} = \sqrt{8 C_d v_{inj} d_{noz}} \frac{1}{2\sqrt{t}} \left(\frac{294}{T_{cyl}}\right)^{1/4} \tag{19}$$

$$v_{wall} = 0.75 \sqrt{v_{inj} d_{noz}} \frac{1}{2\sqrt{t}} \left(\frac{294}{T_{cyl}}\right)^{1/4} \tag{20}$$

In figure 13c, it can be observed that when taking wall impingement into account, the calculated RoHR deviates away from the original model shortly after TDC, staying closer to the measured value. It is also important to note that after EOI, the modelled RoHR decay matches the measured value very closely.

3.1.5 Pilot Combustion model

Pilot injections reduce engine noise, emissions and wear of components by lowering the main ignition delay, lessening the proportion of fuel burnt in a pre-mixed combustion event. For example, the in-cylinder pressure and temperatures prior to the main combustion event are sensitive to the phasing of pilot combustion, since pilot occurs early during the compression stroke, and any errors become cumulative after that point. The effect on pressure is demonstrated in figure 5, comparing the modelled pressure with the correct pilot phasing (solid) to pressure traces where the ignition delay has been artificially altered (dotted) against measured data (dashed).

By necessity pilot injections occur early in the compression stroke, and often have large ignition delays. Therefore, the pilot combustion event is modelled as a fully pre-mixed reaction, since the fuel injection quantities are small and

the fuel air mixture is assumed to be fully mixed prior to combustion [26]. The effect on main injection ignition delay can be modelled by modifying the Arrhenius rate, as proposed by Rether et al [28]:

$$\frac{1}{\tau_{ch}} = C_{arr} c_f c_o e^{-\frac{a_2 T_i}{T + a_4 Q_{pilot}}} \qquad (21)$$

In this case, an additional term is added to the denominator of the exponent proportional to the energy released from the pilot combustion, Q_{pilot}.

3.1.6 Fuel injection model

A requirement for calculating the RoHR using the zero-dimensional model, is accurate prediction of the rate of injection (ROI) [26]. However, since a direct measure of the injection rate is not possible and the objective of this modelling was to be used in HiL applications, it was necessary to develop a Rate of Injection (ROI) model based on mean cycle measured fueling and measured injector current.

The fuel injector used in this study uses a solenoid actuated valve which controls a "spill" flow of fuel through a control chamber back to the vehicle fuel tank. The spill flow creates a pressure imbalance on the injector needle causing the needle to rise, allowing flow through the nozzles into the cylinder. The main difficulty with this type of injector is in knowing when the injector needle is open as this cannot be deduced directly from an injector driver voltage or current. Both the point at which the needle open and the needle opening times must be determined. Figure 6 shows a typical solenoid energizing signal captured using a current clamp around the injector drive cable. The signal can be broken up into three main components, the cracking current (a); hold current (b); and the current fall (c) [30].

Figure 7 compares calculated and measured total fuel injection. The total fuel injected has been calculated by integrating the flow rate over different portions of the injection signal and assuming full needle lift over this proportion. It shows that using any part of the signal up to its entirety correlates linearly with the measured injected quantity above quantities of 25mg. Regardless of the proportion of the signal used, the injected quantity is always underestimated using this method with injection quantities over 25mg. This suggests that either the injection does not occur only over the specific periods defined in figure 6, or that the rate of injection is underestimated.

Below 25mg the relationship changes, suggesting the rate of injection reduces at lower loads, possibly due to needle lift being partial for a significant portion of the injection. This results in the over-estimation of total fuel flow for some points below 25mg.

When the needle is open, the driving force for fuel flow into the cylinder is the pressure difference between the fuel in the common rail and the gases in the cylinder. Flow rate was calculated assuming Bernoulli flow as described in equation 22.

$$\dot{m}_f = C_d \rho_f A_{noz} \sqrt{\frac{2(p_{rail} - p_{cyl})}{\rho_f}} \tag{22}$$

Where the discharge coefficient is modified for the effects of cavitation with C_c the contraction coefficient dependent on the geometry of the injector [31].

$$C_d = C_c \sqrt{\frac{p_{rail} - p_{f,vap}}{p_{rail} - p_{cyl}}} \tag{23}$$

To provide a model with short calculation times, firstly the needle opening duration was determined using an empirical model based on the manufacturer's injector map shown in figure 8. The data in figure 8 was used to estimate the total mass of fuel to be injected depending on the pulse width and the rail pressure.

Inconsistencies could exist between the manufacturer data in figure 8 and the actual injector used in the engine in this study due to injector drift, manufacturing tolerances and engine versions. To account for these, linear functions were applied to rail pressure and pulse width and a quadratic function was applied to the map data. Since injector maps are at atmospheric conditions, a linear correction factor proportional to cylinder pressure was added to simulate the increasing resistance to injection at higher gas loads. Therefore the injector map in figure 8 was incorporated into the model using equation 24. For this look-up table, pulse width was found by integrating the time between the start of the hold current and the end of the hold current (b and c in figure 6).

$$m_{f,pred} = a_5 m_{f,lookup}^2 + a_6 m_{f,lookup} - (a_7 p_{cyl} + a_8) \tag{24}$$

$$Where: m_{f,lookup} = f(t_{pulse}, p_{rail,mod}),$$

$$t_{pulse} = a_9 t_{pulse} + a_{10}$$

$$and\ p_{rail,mod} = a_{11} p_{rail} + a_{12}$$

With a total mass injected (equation 24) and the rate of injection (equation 22), the injection duration between SOI and End of Injection (EOI) was determined from equation 25.

$$m_{f,pred} = \int_{SOI}^{EOI} \dot{m}_f(t)dt \qquad (25)$$

Secondly the point at which the needle lifts and the injection begins (SOI) was determined by analyzing the results from the full hydraulic model and by comparing measured injector current signals and high frequency fluctuation in the high pressure fuel rail in proximity of the injector. This experimental technique assumes that any fluctuations in rail pressure result from the flow of fuel into the cylinder. Using both techniques, SOI was found to correspond to a point approximately 0.17ms into the injector current rise for all injections, pilot and main, and regardless of engine operating point as illustrated in figure 9. This point likely to be where the solenoid has fully risen and flow has been established in the control chamber, resulting in a step change in load on the solenoid as fuel pressure pushes against the spring force. This is evidenced by the subtle change in current rise rate after 0.17ms which can occur due to lower electromagnetic forces acting on the solenoid. These results are consistent with those found by other authors [32].

3.2   Other Models

For the purpose of this work, the other key models described by equation 3 are summarized as below. For a more detailed discussion on this aspect the reader is directed to [33].

- Heat loss to combustion chamber walls: The model proposed by Finol et al. [34] was implemented whilst wall temperature was taken from a look-up table using engine speed and load. In practice, this wall temperature could be obtained from measurements or a separate, more elaborate simulation of the thermal behavior.

- Enthalpy flow by blow by: This was modelled as an isentropic discharge through a nozzle connecting the cylinder and crankcase [35] while assuming a constant flow coefficient.

-   Gas properties of the cylinder charge: these are calculated on a crank angle basis, as a function of temperature, and weighted to consider the instantaneous fractions of fresh air, burnt gases and fuel in the cylinder.

3.3 Model Calibration

Optimization of the model parameters was performed using the MATLAB algorithm *'fminsearch'*, which minimizes the target function for a given set of coefficients.

Figure 10 indicates how the algorithm was implemented. Firstly, the algorithm is given an initial set of parameters. From this, it performs a number of sub-iterations, varying each parameter individually to determine how to reduce the output of the target function. In this case, the target function run the model with the supplied parameters returning the sum of square errors (SSE) calculated from comparing the model output to the measured output. The algorithm then assesses the stopping criteria. If the algorithm exceeds a specified number of iterations, or the rate of change of the target function drops below a given value, the algorithm stops. In the first case, this is to stop the algorithm over running, and in the second it is assumed that a minima has been found.

Using this algorithm, a single set of model parameters were found to suit all test points as opposed to a range of parameters for each individual speed load condition which the model would interpolate. Individual sub-models were optimized using different data sets to ensure the phenomena observed at different operating conditions were captured. Figure 11 indicates the regions of the engine map which were used for model optimization, indicating what data were used for individual sub-models.

Model constants for the ignition delay models were found initially by minimizing the SSE between modelled and observed ignition delay for an individual point. This was then extended to a range of points (point a in figure 11) between 20Nm and limiting torque for a single mid-speed, 2500 rev/min, to ensure the model captured the trend of ignition delay with increasing rail pressure (see figure 4). By calibrating the ignition delay models first, this ensured the pre-mixed portion for the RoHR model was approximately correct, since this depends on ignition delay.

The diffusion RoHR model, and pilot model were calibrated using the mid-speed, mid-load point (point b in figure 11). This point was chosen since the RoHR is mainly diffusive but also includes a pilot injection, as shown in figure 12. In this case, model parameters were found by minimizing the SSE between gross RoHR derived from the model and measured data between inlet valve close (IVC) and exhaust valve open (EVO).

The pre-mixed model constants were optimized in a similar fashion, but at a different operating point. A low speed, medium load condition (point c in figure 11) was chosen since the combustion here was characterized by high ignition delay, and RoHR was dominated by pre-mixed combustion.

The wall interaction model was optimized using a high speed, high load condition (point d in figure 11), where the simulation without the wall interaction model was observed to deviate from measured data.

4   EXPERIMETAL SETUP

Experimental data was collected from a 2.0L Diesel engine installed on a transient engine dynamometer facility. Details of the engine are listed in table 1.

Type	Turbocharged diesel
Nb. Cylinders	4
Displacement	1998cc
Stroke	86mm
Bore	86mm
Conrod Length	152mm
Firing Order	1-3-4-2
Compression Ratio	16 (using prototype pistons)
Max Torque	320Nm at 1800-2000rpm
Max Power	95kW at 3800rpm
Fuel Injection	Common rail (1600bar)

Table 1: Engine specifications

Two data acquisition systems were installed: the first was a *CP Engineering Cadet Automation System* monitoring low frequency data at a rate of 20Hz and the second was a *D2T Osiris* system capturing indication data for every 0.1°CA. Table 2 summarizes the key instrumentation used in this study.

Low frequency	
Channel	**Sensor**
Fuel Flow	CP FMS1000 Gravimetric Flow Meter
Air Flow	ABB Sensy flow hot wire flow meter
Gas Pressure	Piezo-resistive pressure transducers

Gas Temperature	k-type thermocouple 1.5mm
Engine Torque	HBM analog torque sensor

High Frequency	
Channel	**Sensor**
In-cylinder pressure	Kistler Piezoelectric Pressure Sensor (Type 6056A) installed in glow plug adaptor
Fuel rail pressure	Kistler Piezoelectric Pressure sensor (Type 4067A) installed on rail supply pipe.
Injector current	Picotech current clamp

Table 2: Summary of key Instrumentation sensors

After an initial warm up period to allow engine coolant, oil and metal temperatures to stabilize, steady state points were taken at steps of 20Nm from 20Nm to the limiting torque curve (LTC) in steps of 500rev/min from 1000rev/min to 4000rev/min. All measurement points are shown on the engine speed/torque map in figure 11. For each operating condition, data was recorded after a 5 minute settling time and averaged over 30 seconds (low frequency data) or 100 cycles (indicated data).

5 RESULTS AND DISCUSSION

5.1 Review of MCC model performance

Figure 13 shows the behavior of the basic MCC model at three different engine loads and 2500 rev/min. Since the MCC model does not consider ignition delay, in each case the model prediction has been shifted to remove any phase shift with the experimental data in order to facilitate the comparison. The first obvious discrepancy between the model and measured data is the lack of pilot combustion at the low and medium load points. This is because the MCC model was developed on a unit injector system, which typically do not have split injection strategies, unlike modern common rail engines.

By comparing rate of injection to start of combustion (SOC), it is clear that in all cases there is significant ignition delay, especially at low load. As a result, at low load, there is a clear distinction between the model and measured data. The MCC model under-predicts the initial peak caused by pre-mixed combustion, and over predicts RoHR after 15ºCA ATDC.

In the medium load case, the MCC model captures the rise and decay of combustion well, with the exception of some over prediction of the peak and phasing error after end of injection.

At high loads, the MCC model tends to over-predict RoHR, as mentioned in the original study [17]. In Figure 13c, the model over estimates the rate during injection after 5 ºCA ATDC, and under-estimates it after injection. By use of the wall impingement model described previously, predicted RoHR is much closer to the measured data. This suggests that in small displacement engines, wall impingement has a significant influence on the RoHR at high loads.

5.2   Performance of enhanced combustion model

The following section compares the simulation against the heat release results derived from the fired steady state map data presented in figure 11.

5.2.1 Injection Modelling

Predicted injection mass was compared against measured fuel consumption data from the fired steady state data as shown in figure 14. Figure 14a shows that the injector model yielded good correlation with the measured fuel consumption, which is confirmed by an excellent R^2 value of 0.99. From figure 14a, model error appears to be more prevalent at both low levels loads and very high loads. At low loads, error can be attributed to increased cyclic variability caused by the engine operating with low mass airflow, close to the smoke limit of the control strategy. At these points, fuel will be limited according to mass airflow and at low speeds cylinder balancing will adjust fuel delivered to each cylinder dynamically. This increase in variability can result in the cyclic data not being representative of the time-averaged fuel flow data since the cycle-averaged injector signal will be skewed towards the median rather than the mean injected quantity.

The increase in spread at higher loads is most likely due to the decrease in time-based resolution with engine speed, since an error ±0.1ºCA is more significant at this point. In addition to this, the injection pressure is greater at higher loads, resulting in a higher sensitivity to smaller errors.

Despite the error observed at these points, the magnitude of error was low overall, with most between ±2mg, as shown in figure 14b.

5.2.2 Heat Release Modelling

Figure 15 compares gross RoHR derived from measured data (solid grey) to RoHR predicted by the model (solid black), with ROI indicated by dotted grey lines. This is done across a number of steady state points from the fired data

set from low speed to high speed (left to right), and low, medium and high loads (top to bottom). All letters in the following paragraphs refer to those in figure 15.

Overall, the model fits the measured data very well, matching the shape and magnitude of RoHR across all the tests points compared. SOC, peak heat release rates and initial rise rates of combustion are all characterized well by the model. The exponential decay of RoHR observed as the rate of prepared fuel being added to the chamber tails off is also captured for both conditions where this is influenced by injection, (g), (h), (k) and (l), and when this is determined by the dynamics of a flame front, i.e. the Arrhenius rate, shown in (a) to (d).

The model has also captured the influence of ignition delay on combustion, with the operating conditions that have large ignition delays, (a), (b), and (e), exhibiting significantly higher proportions of pre-mixed combustion as indicated by the measured data. However, pre-mixed combustion at high engine speeds is not characterized as well, see (d), (h) and (l), since the initial pre-mixed peak is not clear on the simulated RoHR trace. This is thought to be due to the pre-mixed burning rates being optimized to capture low speed behavior.

Wall impingement is also represented very well, damping the peak ROHR and influencing the decay of heat release at full load, see (i) to (l). Some over-prediction is observed at low speeds, which may be due to incomplete combustion not predicted by the model.

Pilot combustion is characterized very well in terms of magnitude and phasing with the exception of (d) where combustion is late and over-predicted in magnitude, and (j) where the peak is under predicted. In the case of (d) the model over predicts pilot ignition delay, resulting in late main SOC and a larger pre-mixed peak than measured. From the measured data, it appears that pilot occurs earlier, but is not complete, with the remaining fuel being carried over to the main combustion event. By comparing (e), (f), (g) and (h), it is clear that the influence of the change in injection timing with increased engine speed is accurately modelled. Despite pilot timing being advanced significantly over these test points, pilot SOC prediction remains consistent with measured data.

5.2.3. Ignition Delay

Figure 16 compares the trend in measured pilot ignition delay from the fired map data (circles) for increasing rail pressure at constant engine speed against predicted ignition delay (line). It indicates that the pilot ignition delay model has captured the effect of increasing rail pressure and load on pilot ignition delay across a wide range of engine speed

points. There is some deviation in 1000rev/min (a) and 3500rev/min (f), where the model over predicts ignition delay, but overall the trend with rail pressure is captured well.

Figure 17 performs the same comparison, but for the main combustion event. It suggests that main ignition delay model yields good prediction in terms of shape and magnitude, particularly between 2000 rev/min (c) and 3500rev/min (f).

However, for low engine speed (a), the model over predicts ignition delay significantly. This may have been due to the filling/emptying model under predicting in-cylinder pressure, leading to unrealistically low temperatures and an over-estimation of combustion delay.

In addition to this, at very high and low speeds, there was difficulty in measuring main SOC, since it was hard to discern pilot burn from main burn, and also to filter out random noise caused by measuring low cylinder pressures (at low engine speed and load), or that caused by the pre-mixed pilot combustion. Therefore, at these points, the measurement of main SOC may be inaccurate which could have caused some of the deviation between the model and the indicated data.

5.2.4. Combustion

Gross indicated mean effective pressure (IMEP) was chosen as an indicator of engine performance, since this only considers the compression and expansion strokes, which are most influenced by combustion. Figure 18 shows a plot of predicted gross IMEP against measured gross IMEP. Prediction was found to be excellent, with little deviation from experimental data except at very low and extremely high loads, suggesting that the combustion model captured fired engine pressure for the majority of the engine speed and load conditions tested.

Table 3 gives an overview of the predictive ability of the model showing R^2 for the cyclic parameters compared. Overall, the model yields good correlation with the parameters analyzed, R^2 values over 0.9 for most parameters. One notable exception is the angle of maximum cylinder pressure α_{max}, which had an R^2 value of 0.744; however, this still indicates good correlation. The improvement made by introducing the injection rate correction due to cavitation (equation 23) over the model without cavitation is indicated by an increase in R^2.

Parameter	R^2

Main injection qty	0.989
Pilot SOC	0.998
Main SOC	0.998
p_{max}	0.989
α_{max}	0.744
HR_{max} w/o injector cavitation)	0.891
HR_{max} (with injector Cavitation)	0.961
$IMEP_{gross}$	0.996

Table 3: Prediction power for selected combustion parameters

Figure 19 shows the trend in peak pressure against break mean effective pressure (BMEP) for constant speed points for measured data (circles) and predicted data (line). It shows that in general, peak pressure prediction from the model is excellent.

Yet, some deviance is observed at high loads and high speed. For example, at 4000 rev/min (g), The peak cylinder pressure, p_{max} is consistently under-predicted which is thought to be a result of the filling and emptying model underestimating initial in-cylinder pressure during intake at this speed. This is consistent with the results from the initial validation of the filling and emptying model against motored data, where mass airflow and peak pressure were underestimated for high speeds.

Figure 20 shows how the measured (circles) and predicted (line) maximum heat release rate varies with BMEP for a set of steady speeds. It shows that maximum RoHR prediction is good compared to the measured trend for most speeds using model #1 (without injection rate modification), but at high speeds it is over-predicted by some margin. The model with cavitation gives similar prediction to the model without, but maximum heat release rates are decreased, staying closer to the measured data, especially for higher engine speeds. The exception to this is at 3500rev/min (f), where maximum heat release is under predicted with cavitation.

Finally, figure 21 shows how the measured (circles) and predicted (line) point of maximum pressure changes according to rising BMEP across the steady engine speeds measured.

Despite the relatively low R^2, point of maximum pressure is still predicted very well with the model reproducing a trend similar to that measured across a range of speeds and loads, including the discontinuity observed between low and high loads between 1500rev/min (b) and 2500rev/min (d). However, for low loads at 3000rev/min (e), the model

over predicts the point of peak pressure significantly. This may be due to the over-prediction of RoHR during the main combustion for low loads at 3000 rev/min, see figure 15c, causing the point of peak pressure to be shifted towards the expansion stroke.

5   CONCLUSIONS

A new RoHR model has been developed, exhibiting a number of enhancements over Chmela's original MCC model. Injection delay and pre-mixed combustion models were introduced which improved model prediction at part-load.

It was found that at high loads, the diffusion combustion rate was over-predicted using the original model. It was proposed that this was due to fuel flow impinging on the wall, slowing the rate of energy input into combustion due to the momentum lost at the wall. By modelling this effect, predictive improvement in peak combustion rates, phasing and decay were witnessed – The model R^2 values across the engine speed/load map for maximum heat release rate was increased from 0.89 to 0.96.

Due to the presence of multiple injections in the test points taken, a pilot combustion model was required. Based on the

assumption that pilot combustion is predominantly pre-mixed, the pilot model was developed from the main pre-mixed model. Additional terms were added to the ignition delay model to model the influence of pilot combustion on the main ignition lag.

A simple injector model was developed to provide injection rate based on the solenoid energizing signal. This yielded an R^2 values for mass of fuel injected per cycle of 0.99, thus enabling the use of the RoHR model without the need for measured ROI data, which can be challenging to measure directly.

An optimization process was used to calibrate a single set of parameters derived from a small set of measured steady state points. The model was shown to characterize RoHR well over the full range of speed and load points. This was reflected in the model's ability to match both pilot and main phasing, and peak heat release rates derived from measured data. High accuracy in prediction of engine performance parameters such as IMEP, p_{max} and α_{max} was also observed with R^2 values of 0.99, 0.99 and 0.74 respectively. This demonstrates the predictive ability of the model without the need for a large set of empirical data, a key advantage over conventional methods.

REFERENCES

1. Hawley, J.G., F.J. Wallace, and S. Khalil-Arya, A fully analytical treatment of heat release in diesel engines. Proceedings of the Institution of Mechanical Engineers Part D-Journal of Automobile Engineering, 2003. 217(D8): p. 701-717.

2. Benajes, J., Lujam, J.M., Bermudez, V. and Serrano, J.R., Modelling of turbocharged diesel engines in transient operation. Part 1: insight into the relevant physical phenomena. Proceedings of the Institution of Mechanical Engineers Part D-Journal of Automobile Engineering, 2002. 216(5): p. 431-441.

3. Rakopoulos, C.D. and Giakoumis, E.G., Review of Thermodynamic Diesel Engine Simulations Under Transient Operating Conditions, SAE 2006 World Congress2006, SAE International Warrendale Pennsylvania USA: Detroit, Michigan.

4. Pacitti, G., Amphlett, S., Miller, P. Norris, R. and Truscott, A., Real-Time, Crank-Resolved Engine Simulation for Testing New Engine Management Systems, SAE Paper Number 2008-01-1006, SAE 2008 World Congress 2008, SAE International Warrendale Pennsylvania USA: Detroit, Michigan.

5. He, Y. and Rutland, C., Application of Artificial Neural Networks for Integration of Advanced Engine Simulation Methods, in ASME ICE Division Fall 2000 Technical Meeting2000, ASME: Peoria, IL.

6. Longwic, R.c., Modelling the Combustion Process in the Diesel Engine With the Use of Neural Networks, in SAE Powertrains, Fuels and Lubricants Meeting 2008, SAE International Warrendale Pennsylvania USA: Rosemont, Illinois.

7. Papadimitriou, L., Silvestri, J., Warner, M. and Despujois, B. , Development of Real-Time Capable Engine Plant Models for Use in HIL Systems, SAE paper number 2008-01-0990, SAE 2008 World Congress, SAE International Warrendale Pennsylvania USA: Detroit, Michigan.

8. Galindo, J., Lujan, J.M., Serrano, J.R. and Hernandez, L., Combustion simulation of turbocharger HSDI Diesel engines during transient operation using neural networks. Applied Thermal Engineering, 2005. 25(5-6): p. 877-898.

9. Wiebe, I., Habempirische Formel fur die Verbrennungsgeschrwindigkeit Verlag der Akademie der Wissenschaften der VdSSR, 1956, Moscow.

10. Watson, N., A.D. Pilley, and M. Marzouk, A combustion correlation for diesel engine simulation, in Automotive Engineering Congress and Exposition1980, SAE International Warrendale Pennsylvania USA: Detroit, Michigan.

11. Miyamoto, N., Chikahisa, T., Murayama, T. and Sawyer, R., Description and analysis of diesel engine rate of combustion and performance using Wiebe's functions, SAE Paper number 850107, SAE International Congress and Exposition 1985, SAE International Warrendale Pennsylvania USA: Detroit, Michigan.

12. Friedrich, I., H. Pucher, and T. Offer, Automatic Model Calibration for Engine-Process Simulation With Heat-Release Prediction, in SAE 2006 World Congress2006, SAE International Warrendale Pennsylvania USA: Detroit, Michigan.

13. Pirker, G., F. Chmela, and A. Wimmer, ROHR Simulation for DI Diesel Engines Based on Sequential Combustion Mechanisms, in SAE 2006 World Congress2006, SAE International Warrendale Pennsylvania USA: Detroit, Michigan.

14. Arrègle, J., Lopez, J.J, Garcia, J.M. and Fenollosa, C., Development of a zero-dimensional Diesel combustion model: Part 2: Analysis of the transient initial and final diffusion combustion phases. Applied Thermal Engineering, 2003. 23(11): p. 1319-1331.

15. Arrègle, J., Lopez, J.J, Garcia, J.M. and Fenollosa, C., Development of a zero-dimensional Diesel combustion model. Part 1: Analysis of the quasi-steady diffusion combustion phase. Applied Thermal Engineering, 2003. 23(11): p. 1301-1317

16. Payri, F., Benajes, J., Gallindo, J. and Serrano, J.R., Modelling of turbocharged diesel engines in transient operation. Part 2: wave action models for calculating the transient operation in a high speed direct injection engine. Proceedings of the Institution of Mechanical Engineers Part D-Journal of Automobile Engineering, 2002. 216(D6): p. 479-493.

17. Chmela, F.G. and Orthaber, G.C., Rate of heat release prediction for direct injection diesel engines based on purely mixing controlled combustion, SAE Paper Number 1999-01-0186, SAE International Congress and Exposition, SAE International Warrendale Pennsylvania USA: Detroit, Michigan.

18. Lakshminarayanan, P.A., Aghav, Y.V., Dani, A.D. and Mehta, P.S., Accurate prediction of the rate of heat release in a modern direct injection diesel engine. Proceedings of the Institution of Mechanical Engineers Part D-Journal of Automobile Engineering, 2002. 216(D8): p. 663-675.

19. Wallace, F.J. and Hawley, J.G., Analysis of the effect of variations in fuel line pressure in high-speed direct injection diesel engines, with high-pressure common rail fuel injection systems on heat release, cylinder pressure, performance, and NOX emissions. Proceedings of the Institution of Mechanical Engineers Part D-Journal of Automobile Engineering, 2005. 219(D3): p. 413-422.

20. Magnussen, B.F. and Hjertager, B.H., On mathematical modeling of turbulent combustion with special emphasis on soot formation and combustion. Symposium (International) on Combustion, 1977. 16(1): p. 719-729.

21. Dec, J.E., A conceptual model of DI diesel combustion based on laser-sheet imaging, in SAE International Congress and Exposition 1997, SAE International Warrendale Pennsylvania USA: Detroit, Michigan.

22. Pirker, G., F. Chmela, and Wimmer, A., ROHR Simulation for DI Diesel Engines Based on Sequential Combustion Mechanisms, in SAE 2006 World Congress2006, SAE International Warrendale Pennsylvania USA: Detroit, Michigan.

23. Chmela, F., Engelmayer, M., Priker, G. and Wimmer, A., Prediction of turbulence controlled combustion in diesel engines in THIESEL 2004 Conference on Thermo- and Fluid Dynamic Processes in Diesel Engines 2004.

24. Stone, R., Introduction to Internal Combustion Engines, 4th Edition, 2012, p328-331, Basingstoke, Macmillan Press LTD, ISBN 978-0-230-57663-6

25. Assanis, D.N., Filipi, Z.S., Fiveland, S.B. and Syrimis, M., A predictive ignition delay correlation under steady-state and transient operation of a direct injection diesel engine. Journal of Engineering for Gas Turbines and Power-Transactions of the ASME, 2003. 125(2): p. 450-457.

26. Chmela, F.G., G.H. Pirker, and Wimmer, A.. Zero-dimensional ROHR simulation for DI diesel engines - A generic approach. in 19th International Conference on Efficiency, Cost, Optimization, Simulation and Environmental Impact of Energy Systems (ECOS 2006). 2006. Aghia Pelagia, GREECE: Pergamon-Elsevier Science Ltd.

27. Wurzenberger, J.C., Bartsch, P. and Katrasnik, T., Crank angle resolved real-time engine simulation – Integratedsimulation toolchain from office to testbed, SAE Paper Number 2010-01-0784, in SAE world congress 2010, SAE International Warrendale Pennsylvania USA

28. Rether, D., Grill, M., Schmid, A. and Bargende, M., Quasi-Dimensional Modeling of CI-Combustion with Multiple Pilot- and Post Injections, SAE Paper Number 2010-01-0150, SAE 2010 World Congress, SAE International Warrendale Pennsylvania USA: Detroit, Michigan.

29. Barba, C., Burktardt, C., Boulouchos, K. and Bargende, M., A phenomenological combustion model for heat release rate prediction in high-speed DI diesel engines with common-rail injection, SAE Paper Number 2000-01-2933, SAE International Fall Fuels and Lubricants Meeting and Exhibition 2000, SAE International Warrendale Pennsylvania USA: Baltimore, MD.

30. Guerrassi, N. and Dupraz, P., A common rail injection system for high-speed, direct-injection diesel engines, SAE International Congress and Exposition, SAE International Warrendale Pennsylvania USA: Detroit, Michigan.

31. Desantes, J. M., Payri, R., Salvador, F.J. and Gimeno, J., Measurements of Spray Momentum for the study of cavitation in Diesel injection Nozzles, SAE Paper number 2003-01-0703, SAE World Congress 2003, SAE International, Warrendale, Pennsylvania. USA

32. Van Alstine, D. G. Kocher, L.E., Koeberlein, E. and Shaver, G., Control-Oriented Premixed Charge Compression Ignition Combustion Timing Model for a Diesel Engine Utilizing Flexible Intake Valve Modulation, in International Journal of Engine Research, published online 20 August 2012, DOI: 10.1177/1468087412455606

33. Dowell, P.D., Real time heat release model of a HSDI Diesel engine, PhD Thesis, 2012, Dept. of Mechanical Engineering, University of Bath, Bath

34. Finol, C.F., Heat transfer investigations in a modern Diesel engine, PhD Thesis, 2008, Dept. of Mechanical Engineering, University of Bath, Bath

35. Lapuerta, M., Armas, O. and Hernandez, J.J., Dignostics of DI Diesel Combustion from in-cylinder pressure signal by estimation of mean thermodynamic properties of the gas, Applied Thermal Engineering, 19 (5), pp.513-529, 1999
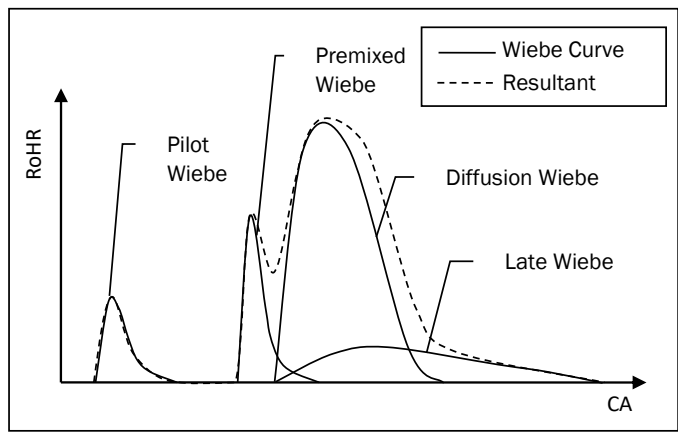
Figure 1: Combustion modelling using Multiple Wiebe approach to capture Rate of Heat Release profile for multiple

injection events
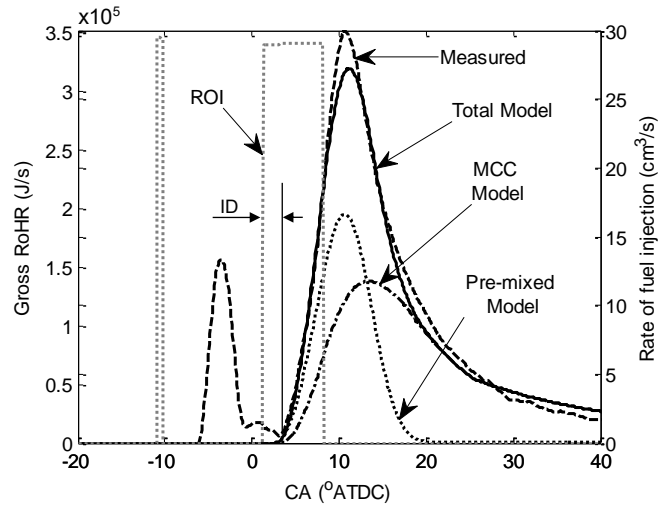
Figure 2: Simulated Rate of Heat Release showing pre-mixed and diffusion (Mixed Controlled) combustion and ignition

delay

ID: Ignition Delay, ROI: Rate of Injection, MCC: Mixing Controlled Combustion
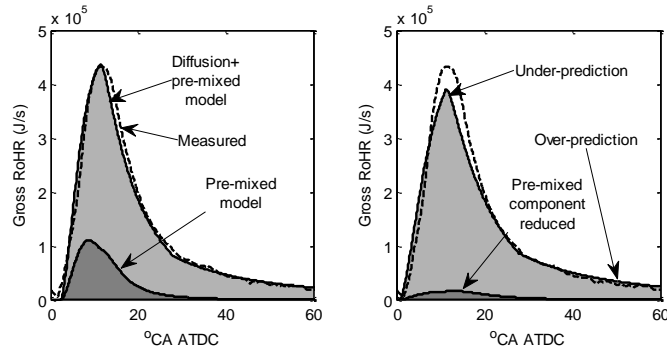
Figure 3: Sensitivity of main combustion profile to combustion phasing: (a) Correct SOC (b) early SOC
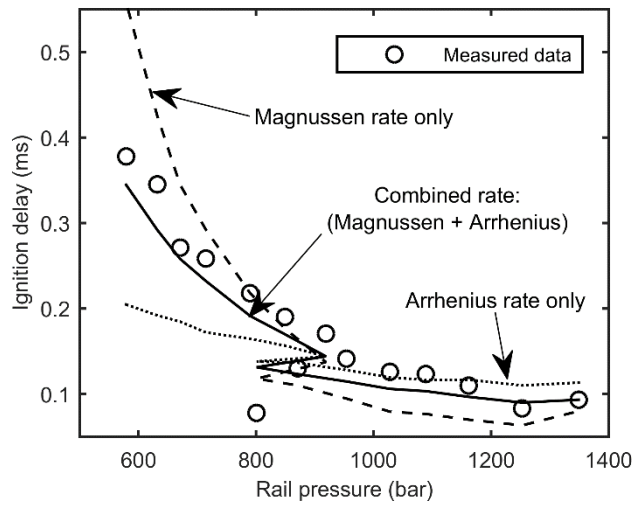
Figure 4: Comparison of ignition delay for Arrhenius, Magnussen and combined models and experimental data. Curves

and measured data represent points obtained from an engine load sweep at 2500rev/min
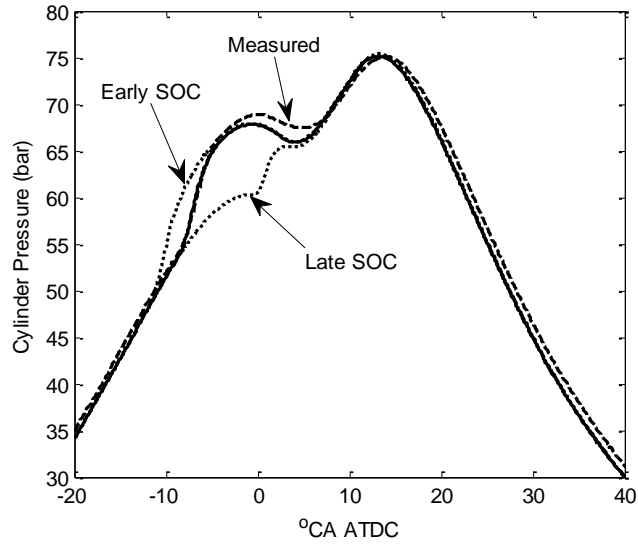
Figure 5: Sensitivity of in-cylinder pressure to the phasing of pilot injection for an arbitrary operating point
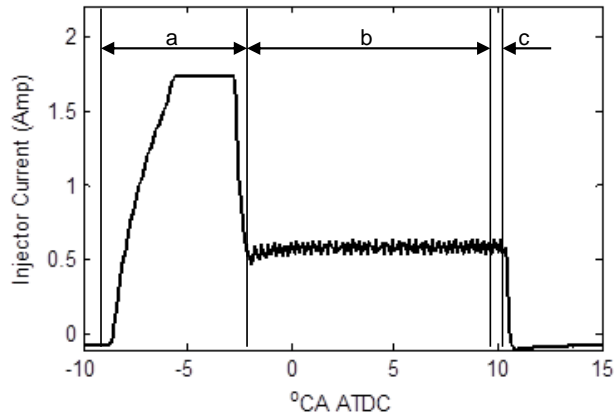
Figure 6: Injector driver current split into three characteristic phases (a= rise / cracking, b= hold, c= fall)
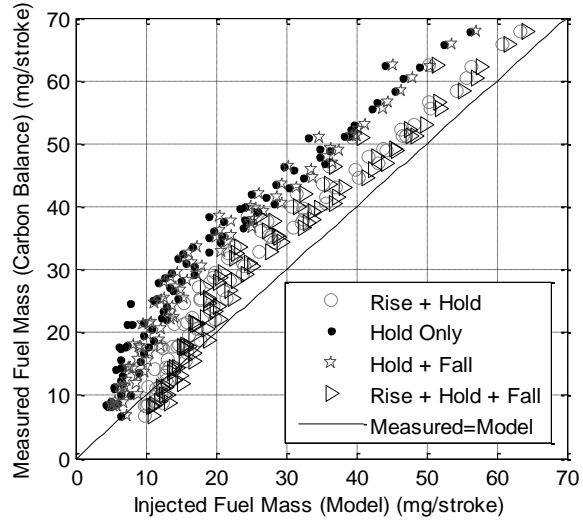
Figure 7: Correlation of measured fuel consumption to predicted fuel injected during various injector current phases
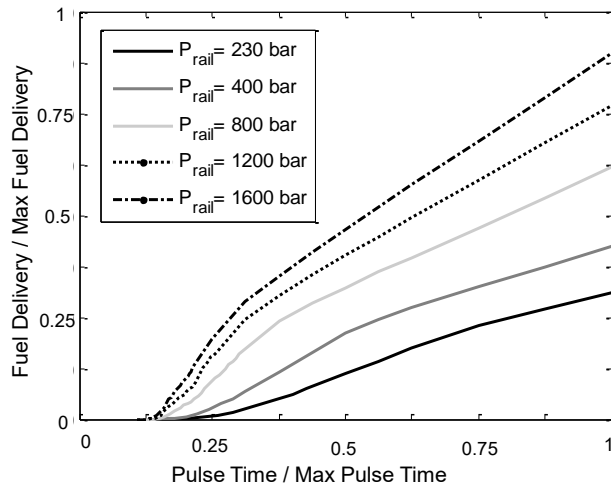
Figure 8: Normalized fuel injection map for Diesel injector
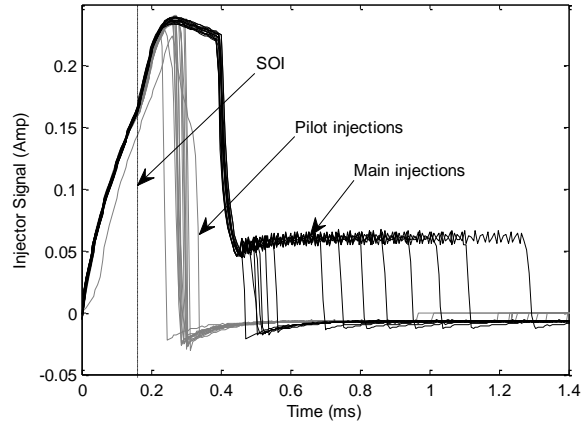
Figure 9: Measured injector currents for pilot and main injections at all engine loads at 2500rev/min
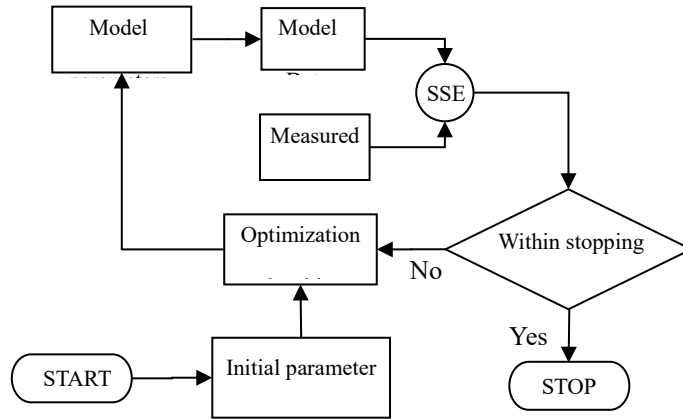
Figure 10: Model parameter optimization routine
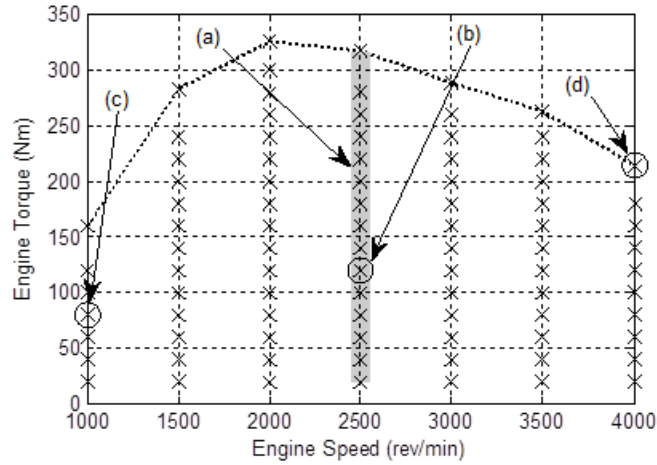
Figure 11: Measured operating points highlighting subsection of points used in model parameter optimization routines for

(a) ignition delay, (b) diffusion combustion, (c) pre-mixed combustion and (d) wall impingement
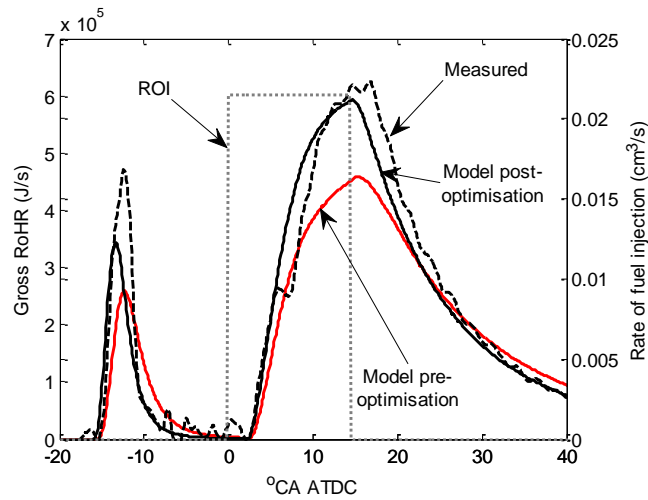
Figure 12: RoHR evolution during the optimization process for engine operating condition of 2500rpm and 125Nm
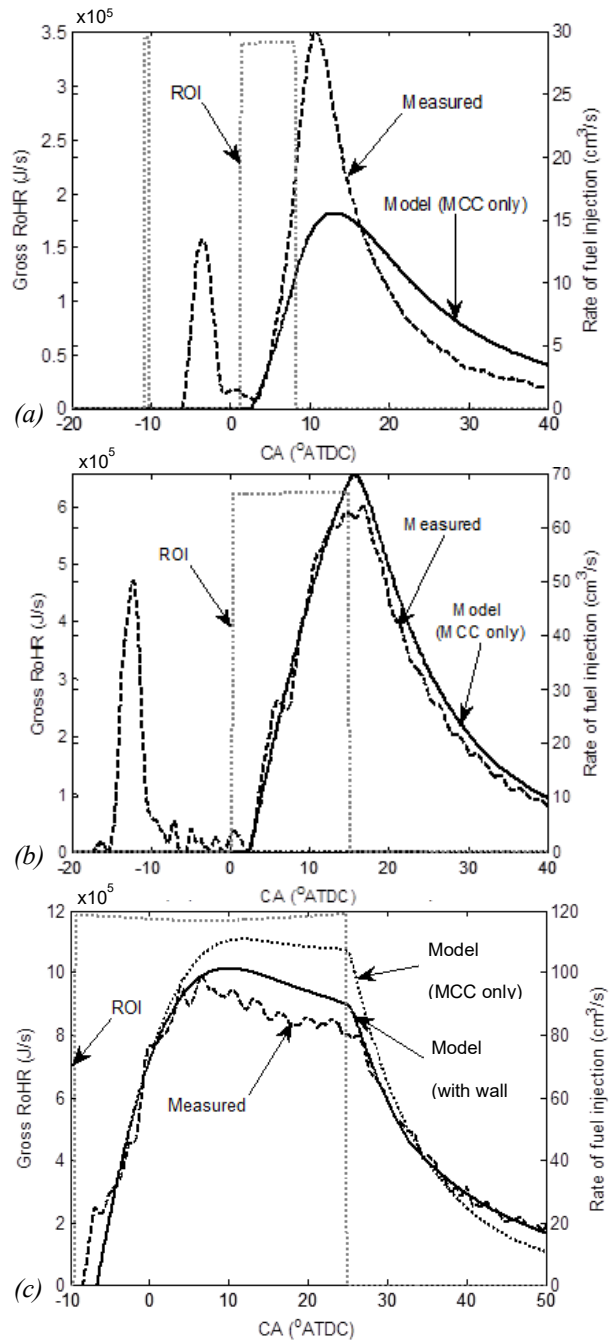
Figure 13: Simulated RoHR using MCC model only at 2500rev/min for (a) low load, (b) medium load and (c) Full load

(a) *(b)*
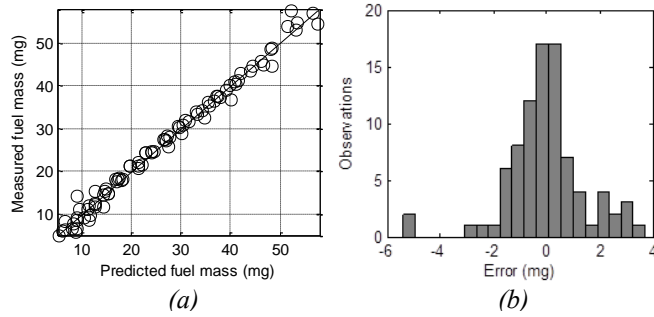
Figure 14: (a) Predicted vs. measured and (b) Prediction error for main injection fuel mass
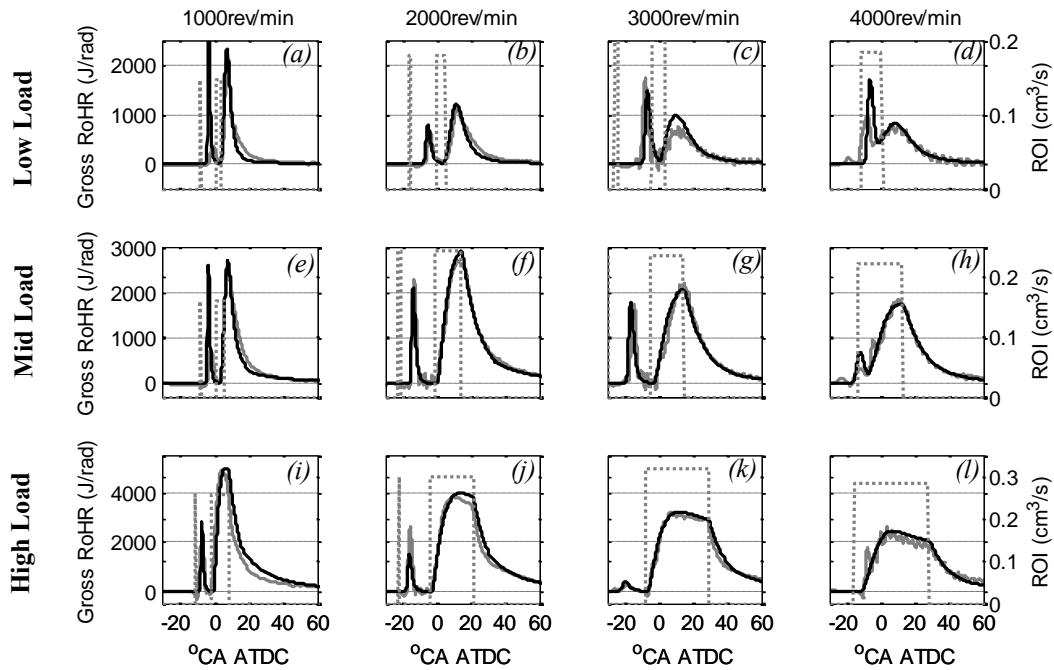
Figure 15: Predicted gross heat release (black solid lines) compared to measured

gross heat release (grey solid lines) with ROI indicated by the grey dotted lines for a

range of engine speeds and loads
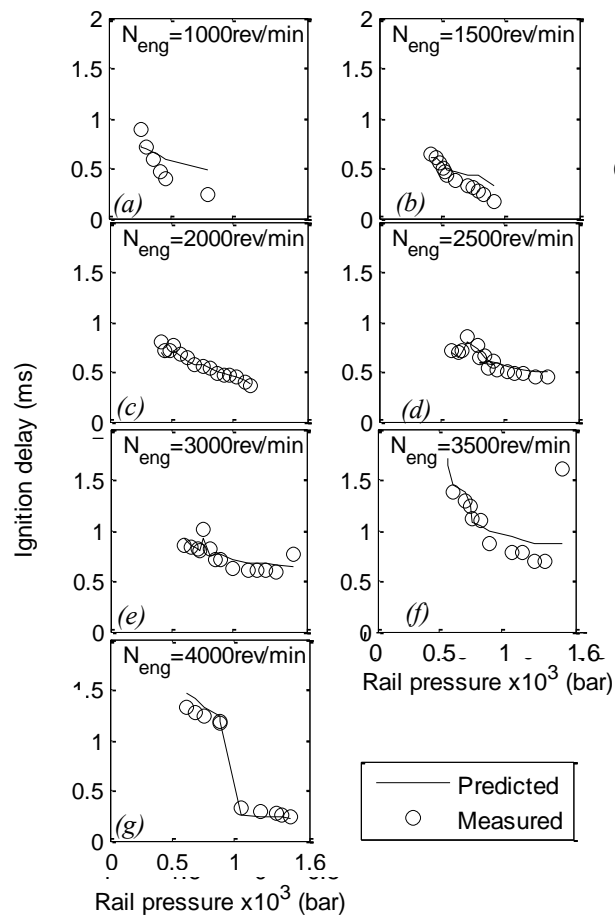
Figure 16: Measured and predicted pilot injection ignition delay grouped by operating speeds
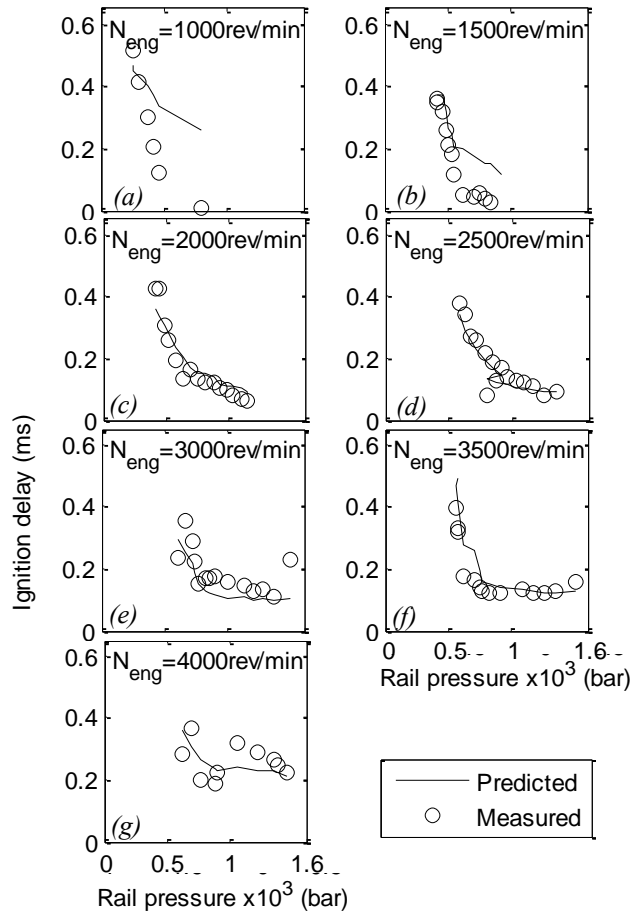
Figure 17: Measured and predicted main injection ignition delay grouped by operating speeds
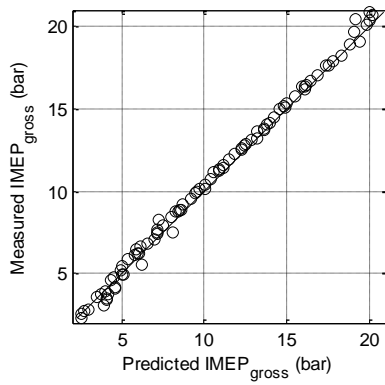
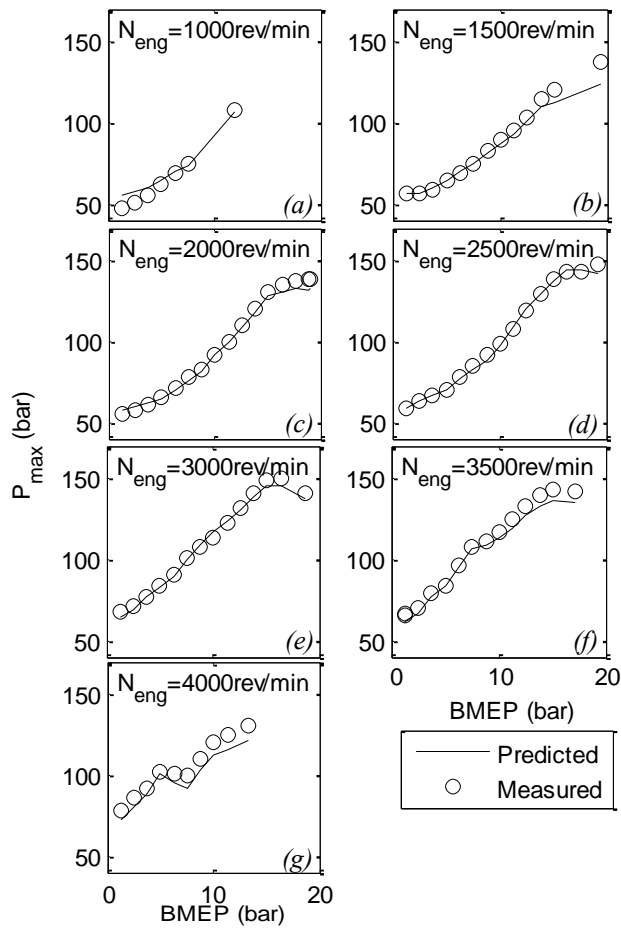**Figure 18: Predicted vs. measured gross IMEP for all test points**

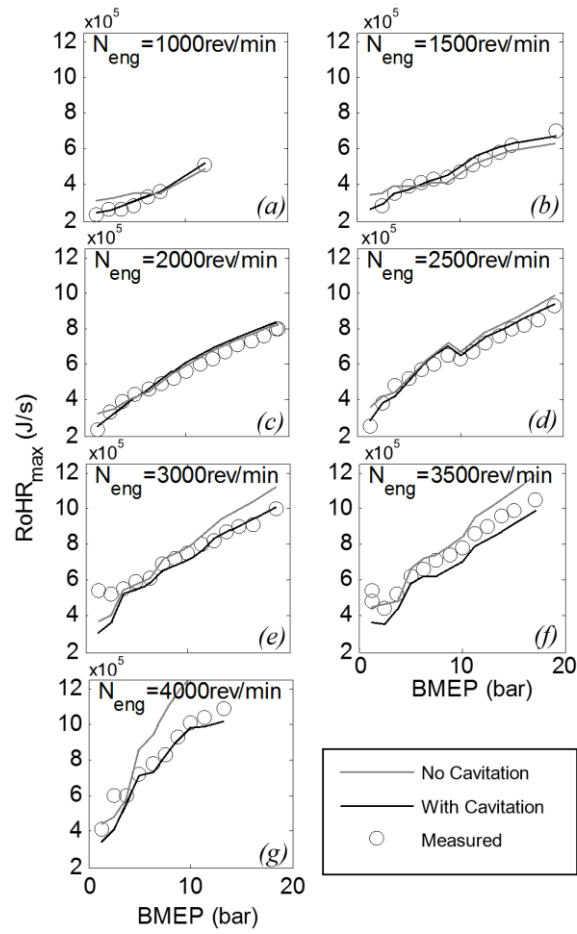**Figure 19: p_{max} prediction vs. measured across different load points**

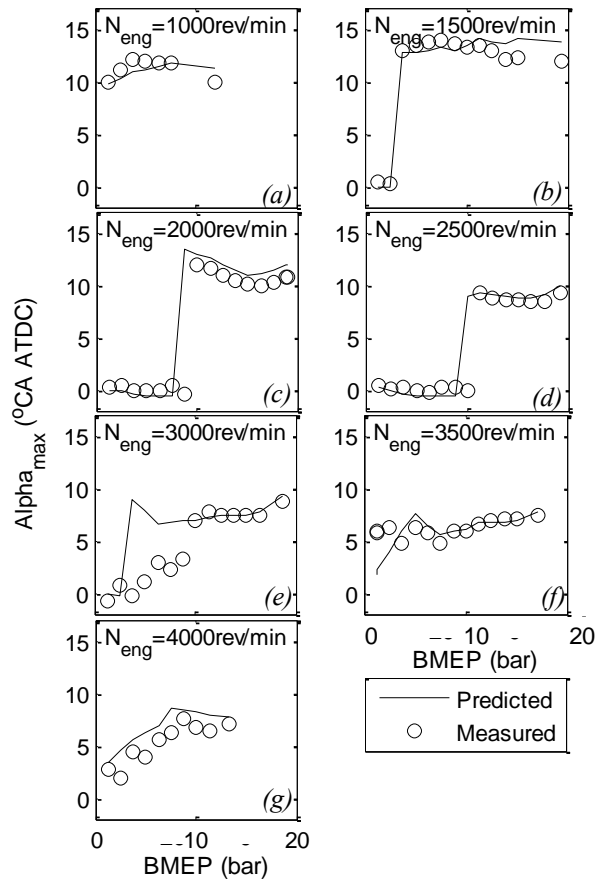**Figure 20: RoHR$_{max}$ prediction against measured across different load points**

Figure 21: Predicted point of maximum pressure against measured across different load points